Synthesis and Preclinical Evaluations of 2-(2-Fluorophenyl)-6,7-methylenedioxyquinolin-4-one Monosodium Phosphate (CHM-1−P-Na) as a Potent Antitumor Agent

Li-Chen Chou,[†] Chien-Ting Chen,[†] Jang-Chang Lee,[†] Tzong-Der Way,[§] Chi-Hung Huang,[‖] Shih-Ming Huang,[†] Che-Ming Teng,[⊥] Takao Yamori,[#] Tian-Shung Wu,[▽] Chung-Ming Sun,[○] Du-Shieng Chien,[◆] Keduo Qian,[‡] Susan L. Morris-Natschke,[‡] Kuo-Hsiung Lee,*,[‡] Li-Jiau Huang,[†,¶] and Sheng-Chu Kuo*,[†,¶]

[†]*Graduate Institute of Pharmaceutical Chemistry, China Medical University, Taichung, Taiwan,* [‡]*Natural Products Research Laboratories, Eshelman School of Pharmacy, University of North Carolina, Chapel Hill, North Carolina 27599-7568,* [§]*School of Biological Science and Technology, China Medical University, Taichung, Taiwan,* [‖]*Taiwan Advance Biopharm, Inc., 12F, No. 25, Lane 169, Kangning Street, Xizhi City, Taipei 221, Taiwan,* [⊥]*Pharmacological Institute, College of Medicine, National Taiwan University, Taiwan,* [#]*Division of Molecular Pharmacology, Cancer Chemotherapy Center, Japanese Foundation for Cancer Research, Tokyo 135-8550, Japan,* [▽]*Department of Chemistry, National Cheng Kung University, No. 1, Dasyue Road, Tainan, Taiwan,* [○]*Department of Applied Chemistry, National Chiao-Tung University, Hsinchu, Taiwan, and* [◆]*SunTen Phytotech Co., Ltd. 4F-1, No. 268, Liancheng Road, Jhonghe City, Taipei County 235, Taiwan.* [¶]*L.-J. Huang and S.-C. Kuo contributed equally to this work.*

CHM-1 [2-(2-fluorophenyl)-6,7-methylenedioxyquinolin-4-one] (**1**) has a unique antitumor mechanism of action. However, because **1** has relatively low hydrophilicity, it was evaluated only via ip administration, which is not clinically acceptable. In this study, we synthesized the monosodium phosphate salt (CHM-1−P-Na, **4**) of **1** as a hydrophilic prodrug. Compound **4** was rapidly converted into **1** following iv and po administration and also possessed excellent antitumor activity in a SKOV-3 xenograft nude mice model. Compound **4** also had clear-cut pharmacological effects on enzymes related with tumor cells. Neither **4** nor **1** significantly affected normal biological function in a safety pharmacology profiling study. Compound **1** caused apoptotic effects in breast carcinoma cells via accumulation of cyclin B1, and importantly, the endogenous levels of the mitotic spindle checkpoint proteins BubR1 directly correlated with cellular response to microtubule disruption. With excellent antitumor activity profiles, **4** is highly promising for development as an anticancer clinical trials candidate.

Introduction

In our prior studies,[1−14] substituted 2-phenylquinolin-4-ones (2-PQs) (Figure 1A) were identified as novel antimitotic agents, and their structure−activity relationships were established from experimental results of numerous related synthetic analogues. Many of the tested 2-PQ derivatives demonstrated potent cytotoxicity against human cancer cell lines and were selected for in vivo testing in our laboratory. To date, among tested compounds, 2-(2-fluorophenyl)-6,7-methylenedioxyquinolin-4-one (CHM-1,[a] **1**) (Figure 1B) has been identified as the most active compound in vivo. Namely, when **1** was evaluated in SCID mice bearing HA-22T xenograft, the tumor growth was remarkably suppressed and the survival life span was significantly extended by **1** at a dosage of 10 mg/kg injected intraperitoneally (ip) Q4D × 3 when compared with the control group.[15] Compound **1** was also evaluated against OVCAR-3 ovarian tumor xenograft in nude mice by the National Cancer Institute (NCI, USA) and was found to exhibit excellent antitumor activity. At dosages of 200, 134, and 79 mg/kg (Q7D × 3, ip), **1** extended the life span of tumor-bearing mice by 124%, 133%, and 79%, respectively. Notably, even at the highest test dosage (200 mg/kg), **1** did not reach the maximum tolerance dose (MTD). The preliminary results from the above in vivo studies clearly indicate that **1** has significant antitumor activity while maintaining low toxicity. Unfortunately, **1** has relatively low water solubility (13 ng/mL); thus, its animal study could only be done via ip administration, which is not suitable for clinical use. Accordingly, to enhance the developmental value of **1**, we designed its conversion to a prodrug, which could be administrated through both oral and iv routes.

In the present study, we selected the hydrophilic monosodium phosphate of **1** (CHM-1−P-Na, **4**) (Figure 1B) as the target compound. This prodrug should be converted readily to the parent molecule in the bloodstream or gastrointestinal tract by reaction with nonspecific alkaline or acidic phosphatases.[16−20] Similar prodrug strategies have successfully improved the clinical usage of estramustine, etoposide, combretastatin A-4, and 2-methoxyestradiol.[21−25]

Recently, enzyme-mediated cancer imaging and therapy (EMCIT)[26−29] has been developed as a novel method for enzyme-dependent, site-specific in vivo precipitation of

---

*To whom correspondence should be addressed. For K.-H.L.: phone, 919-962-0066; fax, 1-919-966-3893; E-mail: khlee@unc.edu. For S.-C. K.: phone, +886-4-22053366-5608; fax, +886-4-22030760; E-mail: sckuo@mail.cmu.edu.tw.

[a] Abbreviations: CHM-1, 2-(2-fluorophenyl)-6,7-methylenedioxyquinolin-4-one; CHM-1-P, 2-(2-fluorophenyl)-6,7-methylenedioxyquinolin-4-one dihydrogen phosphate; CHM-1-P-Na, 2-(2-fluorophenyl)-6,7-methylenedioxyquinolin-4-one monosodium phosphate; ip, intraperitoneal; iv, intravenous; po, oral; SPP, safety pharmacology profiling; MTD, maximum tolerance dose; EMCIT, enzyme-mediated cancer imaging and therapy; JFCR, Japanese Foundation for Cancer Research; AUC, area under curve; ADME, administration, distribution, metabolism, excretion; PQ, phenylquinolone.
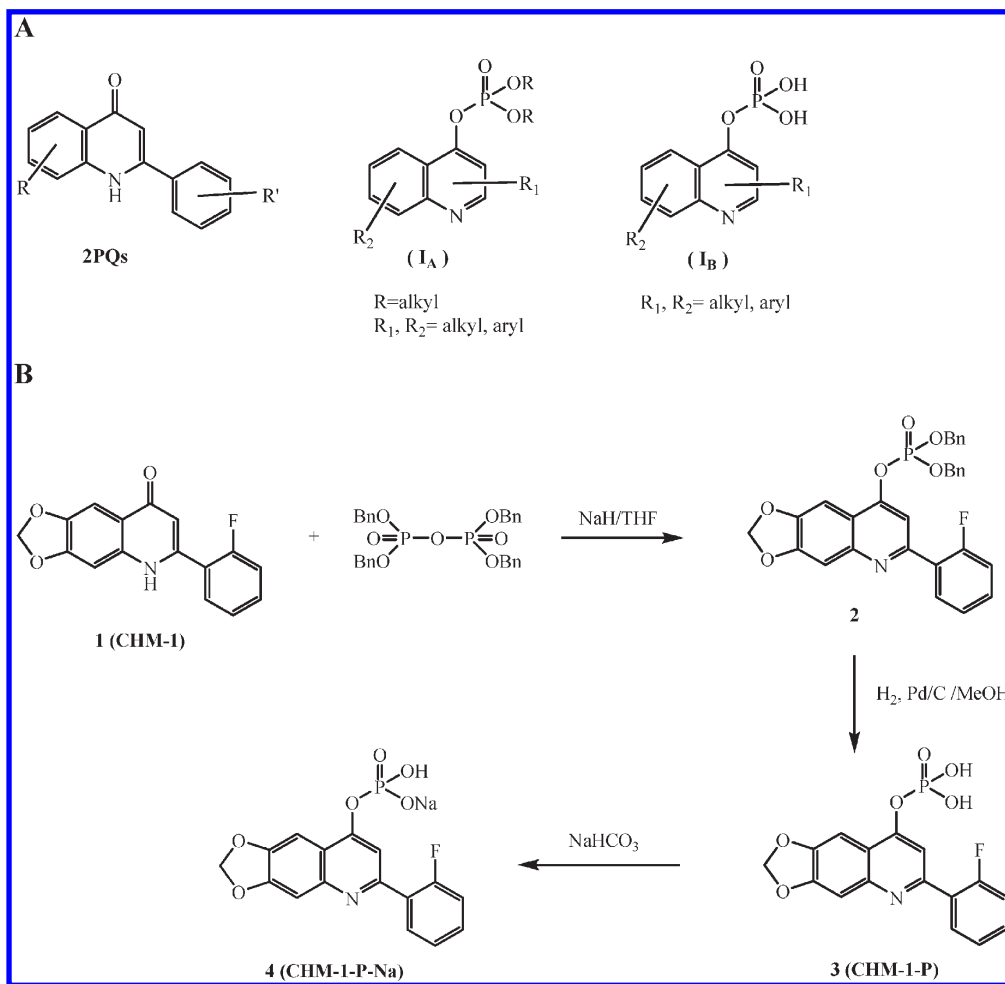
Figure 1. (A) Structures of substituted 2-phenylquinolin-4-ones (2-PQs). (B) Synthesis of sodium 2-(2-fluorophenyl)-6,7-methylenedioxy-quinolin-4-yl hydrogen phosphate (**4**).
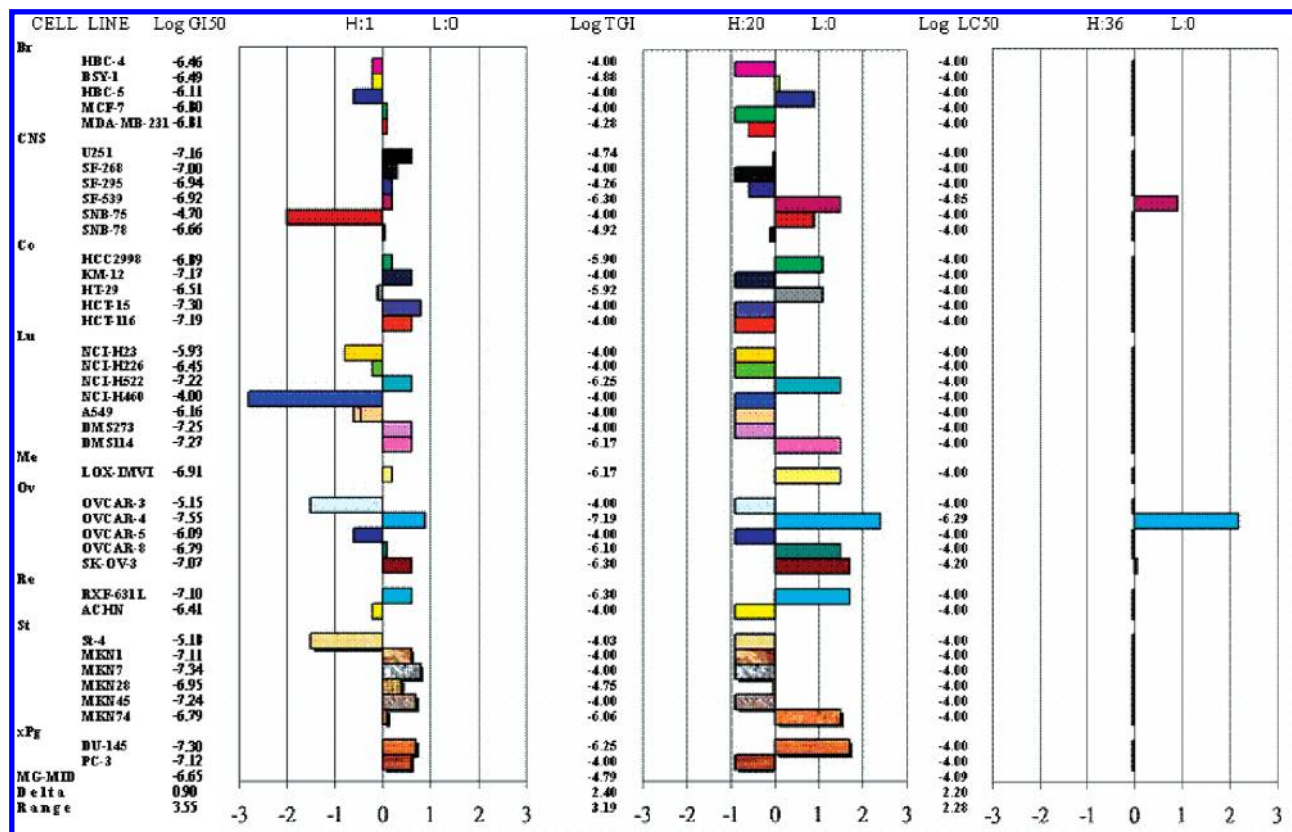
water-insoluble radioactive molecules within solid tumors. A radiolabeled prodrug containing a phosphate moiety is dephosphorylated both in vitro and in vivo to its water-insoluble form by alkaline phosphatase overexpressed on the extracellular space of some specific tumor cells, such as ovarian, bladder, and hepatoma cells. On the basis of this methodology, we were encouraged to pursue the synthesis of **4** as a reasonable target delivery strategy. Our phosphate-bearing prodrug, **4**, could reasonably be desphosphorylated to its water-insoluble form and precipitated in situ on the extracellular space of SKOV-3 ovarian tumors. In this paper, we report the synthesis of **4** and the selective toxicity of **1** against various human cancer cell lines. Also reported are the results of a preliminary pharmacokinetic study and evaluation of the antitumor activity of **4** following oral and iv administration.

Safety pharmacology profiling (SPP) is a reliable, fast, and cost-effective means for determining potential drug liabilities to aid lead selection and lead optimization. Analysis of profiling data enables us to find off-target interactions for predicting potential side-effects, efficacy, and safety of compounds. SPP concentrates on early hazard identification to guide drug discovery projects and to minimize or abolish deleterious effects through structure−activity relationship considerations. Early compound profiling by in vitro pharmacology profiling can flag for receptor-, enzyme-, transporter-, and channel-related liabilities of compounds and translates these data into conjunction with ADME and

toxicity (ADME−Tox) characteristics. Therefore, we can use enzyme and radioligand binding assays to identify targets associated with beneficial effects for treating cancer or with possible side effects. Both **1** and **4** were evaluated, and their safety profiling results were recorded. The mechanism of action of **4**'s antitumor activity was also explored and reported in the current study.

Chemistry

Although the synthesis of monosodium phosphate salt of **1** was challenging due to the ready decomposition of CHM-1-phosphate (**3**) back to **1** in MeOH, it was successfully achieved. Although synthetic methods to produce quinolin-4-phosphoric acid dialkyl esters (**I$_A$**) (Figure 1A) have been reported,[3,30] a literature search revealed no information about the preparation of the hydrolyzed quinolinol-4-phosphoric acids (**I$_B$**) (Figure 1A). To our knowledge, this is the first time that phosphate has been linked to the 4-*O* position of a quinoline. The synthesis of 2-(2-fluorophenyl)-6,7-methylene-dioxyquinolin-4-yl phosphate monosodium salt (**4**) is illustrated in Figure 1B. Initially, **1** was dissolved in THF, and reacted with tetrabenzyl pyrophosphate in the presence of NaH, to yield dibenzyl 2-(2-fluorophenyl)-6,7-methylene-dioxyquinolin-4-yl phosphate (**2**). Compound **2** was subjected to Pd/C catalytic hydrogenolysis in MeOH to give **3** in high yield (97%). The compound precipitated from solution, which prevented the further decomposition of the prodrug. Finally,

CELL LINE		Log GI50	Log TGI	Log LC50
Br	HBC-4	-6.46	-4.88	-4.00
	BSY-1	-6.49	-4.88	-4.00
	HBC-5	-6.11	-4.00	-4.00
	MCF-7	-6.80	-4.00	-4.00
	MDA-MB-231	-6.81	-4.28	-4.00
CNS	U251	-7.16	-4.74	-4.00
	SF-268	-7.00	-4.00	-4.00
	SF-295	-6.94	-4.26	-4.00
	SF-539	-6.92	-6.30	-4.00
	SNB-75	-4.70	-4.00	-4.85
	SNB-78	-6.66	-4.92	-4.00
Co	HCC2998	-6.89	-5.90	-4.00
	KM-12	-7.17	-4.00	-4.00
	HT-29	-6.51	-5.92	-4.00
	HCT-15	-7.30	-4.00	-4.00
	HCT-116	-7.19	-4.00	-4.00
Lu	NCI-H23	-5.93	-4.00	-4.00
	NCI-H226	-6.45	-4.00	-4.00
	NCI-H522	-7.22	-6.25	-4.00
	NCI-H460	-4.00	-4.00	-4.00
	A549	-6.16	-4.00	-4.00
	DMS273	-7.25	-4.00	-4.00
	DMS114	-7.27	-6.17	-4.00
Me	LOX-IMVI	-6.91	-6.17	
Ov	OVCAR-3	-5.15	-4.00	-4.00
	OVCAR-4	-7.55	-7.19	-6.29
	OVCAR-5	-6.09	-4.00	-4.00
	OVCAR-8	-6.79	-6.10	-4.00
	SK-OV-3	-7.07	-6.30	-4.20
Re	RXF-631L	-7.10	-6.30	-4.00
	ACHN	-6.41	-4.00	-4.00
St	St-4	-5.18	-4.03	-4.00
	MKN1	-7.11	-4.00	-4.00
	MKN7	-7.34	-4.00	-4.00
	MKN28	-6.95	-4.75	-4.00
	MKN45	-7.24	-4.00	-4.00
	MKN74	-6.79	-6.06	-4.00
xPg	DU-145	-7.30	-6.25	-4.00
	PC-3	-7.12	-4.00	-4.00
MG-MID		-6.65	-4.79	-4.09
Delta		0.90	2.40	2.20
Range		3.55	3.19	2.28

Figure 2. Differential activity patterns for **1** against 39 human cancer cell lines. MG-MID: mean of log X values ($X = GI_{50}$, TGI, and LC_{50}). Delta: logarithm of the difference between the MG-MID and the log X of the most sensitive cell line. Range: logarithm of the difference between the log X of the most resistant cell line and the log X of the most sensitive cell line. H: High concentration (10^{-4} M) (highest concentration of **1** used during testing); L: Low concentration (10^{-8} M) (lowest concentration of **1** used during testing). H:1 indicates that the number of cell lines tested at the highest concentration is 1. L:0 indicates that the number of cell lines tested at the lowest concentration is 0.

3 was treated with $NaHCO_3$ to obtain the water-soluble monosodium salt (**4**).

Biology

Growth Inhibitory Activity of 1 against Human Cancer Cell Line Panel. Compound **1**, the parent compound of **4**, was evaluated for its growth inhibitory activity against the JFCR-39 human cancer cell panel by the Japanese Foundation for Cancer Research (JFCR).[31−33] The evaluation was carried out to determine the selective responses of **1** toward various human cancer cell lines so that the results could be used as a guideline for selecting suitable cancer types in the animal study of its prodrug, **4**.

The growth inhibitory activity data of **1** were analyzed computationally and presented as dose−response curves at five different concentrations between 10^{-4} and 10^{-8} M. GI_{50}, TGI, and LC_{50} values were calculated, and the corresponding mean graph or fingerprint (Figure 2) was obtained.

Our results showed that **1** was active against most tested cancer cell lines with a mean log GI_{50} (MG-MID) value of −6.65. In particular, **1** was profoundly cytotoxic (log GI_{50} < −7.0) against the following 15 cell lines: U251, KM-12, HCT-15, HCT-116, NCI-H522, DMS-273, DMS-114, OV-CAR-4, SKOV-3, RXF-631 L, MKN-1, MKN-7, MKN-45, DU-145, and PC-3.

Unique COMPARE Fingerprint of 1. The fingerprint of the preferential responses of **1** against specific cells in the cell panel was then analyzed by a pattern-recognition computer program (COMPARE), which contains a database covering similar types of fingerprints from over 300 known anticancer agents with various mechanisms of action. The low correlation coefficient ($r < 0.4$) found in fingerprint-matching for **1** seemed to imply that its mechanism of action differed widely from those of the anticancer agents covered in the COM-PARE database.

Single Dose Pharmacokinetics of 4 in Male CD-1 (*Crl.*) Mouse. One objective of this study was to find the dosage of **4** required to achieve significant antitumor activity via iv and oral administration. As mentioned above, an ip dose of 10 mg/kg of **1** resulted in significant antitumor activity in our animal study. After the dosing, pharmacokinetic parameters were determined. Similarly, 10 mg/kg of the prodrug **4** was administered via iv and oral routes, and the pharmacokinetic parameters of **3** and its metabolite **1** were determined. The dosage of **4** required to achieve significant antitumor activity in an animal study could thus be predicted by comparing the pharmacokinetic profiles of **1** and **4**.

Selected pharmacokinetic parameters are summarized in Table 1 for ip, iv, and po administration, respectively. The mean plasma concentration−time curves of **1** and **3**, determined after ip, iv, and po dosing, are shown in Figure 3A−D.

As shown in Figure 3A, a high concentration of active metabolite **1** appeared almost instantly in the mouse bloodstream after iv dosing of 10 mg/kg of **4**, while the concentration of prodrug **3** declined rapidly to a very low level within 1 h. These results indicated that **4** was quickly converted into its active parent compound **1** after iv dosing.

The plasma levels of **1** following iv and ip dosing of **4** and **1**, respectively, are shown in Figure 3B. This comparison

Table 1. Pharmacokinetic Parameters of **1** and **4** in Male CD-1 (*Crl.*) Mice Following a Single Dose of either **1** or **4** at 10 mg/kg by Different Routes

compd dosed	compds examined	C_{max} (ng/mL)	AUC(0−inf) (ng·h/mL)	T_{max} (h)	MRT (h)	CL (mL/(min·kg))	$t_{1/2}$[b] (h)
1 (ip)	**1**	155	417	0.3	7.3	nd[a]	7.3
4 (iv)	**3**	29810	3220	nd[a]	0.1	51.7	nd[a]
	1	8702	1956	nd[a]	0.7	nd[a]	1.0
4 (po)	**3**	91	28	0.3	0.3	nd[a]	nd[a]
	1	1312	1230	0.5	1.4	nd[a]	1.0

[a] nd: not determined. [b] $t_{1/2}$ was determined from 6 to 27 h time points.
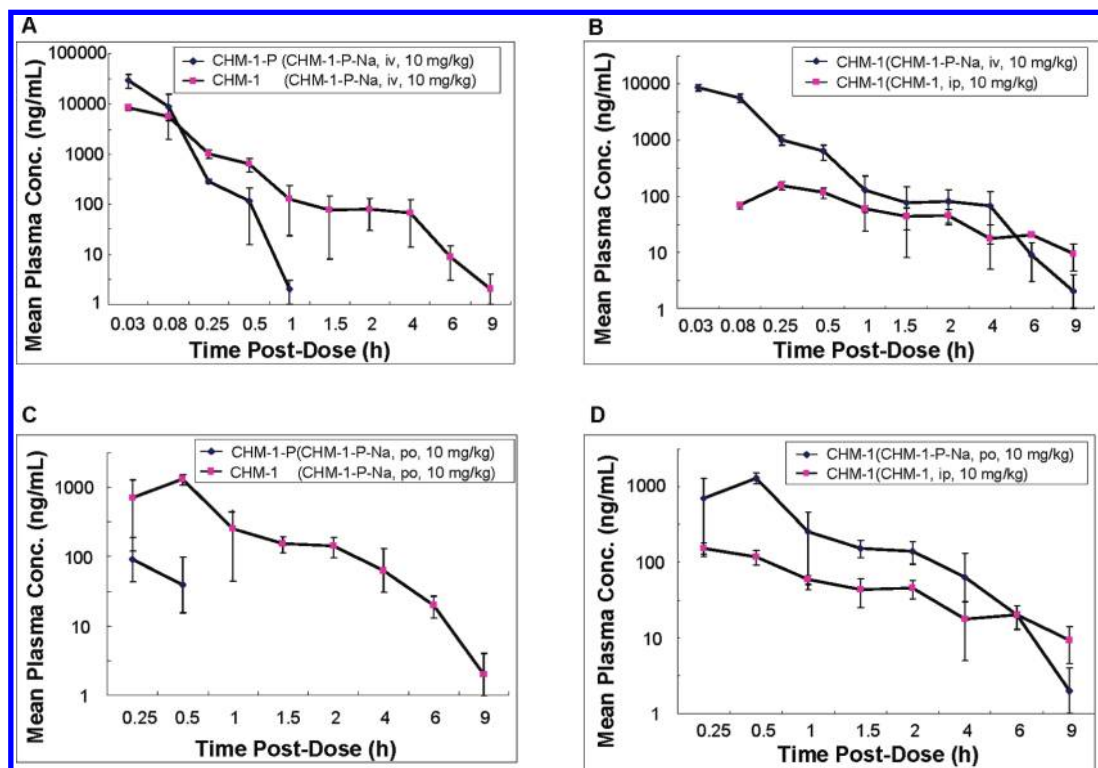
Figure 3. (A) Mean plasma concentration−time profiles of **1** and **4** in male CD-1 (*Crl.*) mice following a single iv dose of **4** at 10 mg/kg. (B) Mean plasma concentration−time profiles of **1** in male CD-1(*Crl.*) mice following a single iv dose of **4** and single ip dose of **1** at 10 mg/kg. (C) Mean plasma concentration−time profile of **1** and **3** in male CD-1 (*Crl.*) mice following a single po dose of **4** at 10 mg/kg. (D) Mean plasma concentration−time profiles of **1** in male CD-1 (*Crl.*) mice following a single po dose of **4** at 10 mg/kg and single ip dose of **1** at 10 mg/kg.

indicated that the plasma concentration of **1** (AUC = 1956 ng·h/mL, Table 1) following iv dosing of **4** was significantly higher than that of **1** (AUC = 417 ng·h/mL, Table 1) following ip dosing of **1**, particularly in the first hour postdosing. Therefore, we expected that the antitumor activity of **4** at 10 mg/kg iv dosing would be superior to that resulting from **1** at 10 mg/kg ip dosing.

Meanwhile, as shown in Figure 3C, after po dosing of 10 mg/kg of **4**, the plasma concentration−time profiles of **3** and its metabolite **1** appeared to follow the same pattern (Figure 3A) found with iv dosing of **4**. Namely, the active metabolite **1** appeared instantly in the bloodstream, while the concentration of **3** declined rapidly until it essentially disappeared within an hour. This experiment demonstrated that **4** was also quickly converted into its active metabolite **1** following oral dosing.

Figure 3D compares the pharmacokinetic profiles of **4** and **1** following po and ip dosing, respectively. The plasma concentration of **1** (AUC = 1230 ng·h/mL, Table 1), following oral dosing of **4**, was higher than that of **1** (AUC = 417 ng·h/mL, Table 1) following ip dosing of **1**. Likewise, we

expected that the antitumor activity for **4** at 10 mg/kg po dosing of would be superior to that resulting from **1** at 10 mg/kg ip dosing.

Acute Oral Toxicity of 4. The mortality of male mice orally administered **4** from group 1 to group 5 was 0/5, 0/5, 0/5, 0/5, and 5/5, and of female mice was 0/5, 0/5, 0/5, 2/5, and 5/5, respectively. Dosages of test compound, administered by gavage, were 0, 500, 1500, 2700, and 5000 mg/kg for groups 1−5, respectively. Hunched posture, tremors, and prostration were observed before animals died. Salivation, hypoactivity, soft feces, and feces stain were observed in other surviving animals. All observations were gone within three days. None of the animals had obvious gross lesions. The LD_{50} with 95% confidence interval was 2462 mg/kg in females and 2720 mg/kg in males.

Safety Pharmacology Profiling (SPP) of 1 and 4. To explore their general pharmacological activities, **1** and **4** were further screened in 317 enzyme assays and 167 radioligand binding assays. The results of inhibitory activity screening of **1** are summarized in Table 2. At 10 μM, **1** showed significant responses ($\geq$50% inhibition) toward glutamate

Table 2. Inhibitory Effects of **1** on Enzyme and Radioligand Binding Assays for SPP

biological assay[a]	species	% of inhibition
glutamate decarboxylase[b]	*C. perfringens*	66
monoamine oxidase MAO-A[b]	human	52
peptidase, CTSD (cathepsin D)[b]	human	27
peptidase, CTSE (cathepsin E)[b]	human	12
peptidase, CTSS (cathepsin S)[b]	human	1
peptidase, pepsin[b]	pig	85
CYP450, 2D6[b]	human	nd[d]
protein serine/threonine kinase [MAPK10 (JNK3)][b]	human	55
protein tyrosine phosphatase, PTP4A1(PRL-1)[b]	human	nd[d]
protein tyrosine phosphatase, PTP4A2(PRL-2)[b]	human	nd[d]
protein tyrosine phosphatase, PTP4A3(PRL-3)[b]	human	nd[d]
GABA$_A$, benzodiazepine control[c]	rat	83
GABA$_A$, flunitrazepam, central[c]	rat	nd[d]

[a] Concentration = 10 μM. [b] Enzyme assay. [c] Radioligand binding assay. [d] nd: no determination.

Table 3. Inhibitory Effects of **4** on Enzyme and Radioligand Binding Assays for SPP[a]

biological assay[b]	species	inhibition %	IC$_{50}$ (μM)
glutamate decarboxylase[c]	*C. perfringens*	nd[e]	nd[e]
monoamine oxidase MAO-A[c]	human	−24	nd[e]
peptidase, CTSD (cathepsin D)[c]	human	50	9.79
peptidase, CTSE (cathepsin E)[c]	human	78	1.71
peptidase, CTSS (cathepsin S)[c]	human	106	1.62
peptidase, pepsin[c]	pig	−19	nd[e]
CYP450, 2D6[c]	human	73	3.22
protein serine/threonine kinase [MAPK10 (JNK3)][c]	human	−20	nd[e]
protein tyrosine phosphatase, PTP4A1(PRL-1)[c]	human	98	0.676
protein tyrosine phosphatase, PTP4A2(PRL-2)[c]	human	101	0.314
protein tyrosine phosphatase, PTP4A3(PRL-3)[c]	human	72	4.93
GABA$_A$, benzodiazepine control[d]	rat	nd[e]	nd[e]
GABA$_A$, flunitrazepam, central[d]	rat	62	5.57

[a] A standard error of the means is presented where results are based on multiple, independent determination. [b] Concentration = 10 μM. [c] Enzyme assay. [d] Radioligand binding assay. [e] ND: no determination.

decarboxylase, MAO-A, pepsin, MAPK10, and GABA$_A$. The same screening indicated that **4** exhibited significant inhibitory activity against eight targets at 10 μM, and further assessment was performed to determine IC$_{50}$. The inhibitory activity of **4** was greatest against protein tyrosine phosphatases PRL-1 and PRL-2 (IC$_{50}$ < 10.0 μM) (Table 3). Among those enzymes and ligand inhibited by **4**, PRL-1, -2, and -3 are postulated to promote cell motility, invasion, and metastasis, while cathepsin-D, -E, -S, and GABA$_A$ are also associated with tumor activity.[34−38]

In Vivo Antitumor Activity of 4. On the basis of the above cytotoxicity data of **1** and the pharmacokinetic parameters of **4**, we selected the SKOV-3 xenograft model using dosing at 5, 10, and 20 mg/kg (iv and po) to evaluate the in vivo antitumor activity of **4**.

According to the results shown in parts A and B of Figure 4, **4** induced dose- and time-dependent inhibition of SKOV-3 tumor growth. Significant tumor growth suppression was detected at 5 mg/kg/day, and almost complete tumor suppression was observed at 20 mg/kg/day. During the course of antitumor evaluation, no significant body weight changes were detected in either test or control mice (Figure 4C,D).

The above findings indicated that **4** has excellent antitumor activity when administered either iv or po and that the same dosing led to similar antitumor efficacy, regardless of administration route.

Compound 1 Inhibits Cell Growth in Human Ovarian Cancer Cells by Inducing Mitotic Arrest. We first determined the effect of **1** on the growth of ovarian cancer cell lines using the MTT assay. We chose three clinical trial agents, taxol, colchicine, and doxorubicin, as positive controls, and in comparison, **1** had a nearly equivalent effect against cancer cells (Figure 5A). These data indicate that **1** induces potent cytotoxicity in human ovarian cancer cells. To clarify the mechanism of **1**-induced proliferation inhibition, we examined the effect of **1** on the cell cycle. Compound **1** caused the accumulation of cells in the G2-M phase with concomitant losses in G0−G1 phase, with a maximum effect observed at 36 h (Figure 5B). The accumulation of cells with G2-M DNA content was followed by an increase in hypodiploid cells at the later time points (48 h), as indicated as apoptotic cells. These results indicate that **1** induced G2-M arrest of the cell cycle followed by apoptosis. To better understand the mechanism of **1**-induced G2-M arrest, the expression of cell cycle−related proteins was analyzed. Cyclin B1 and securin serve as markers for mitotic arrest induction. Accordingly, we next assessed the effects of **1** on cyclin B1 and securin protein expression. Treatment of SKOV-3 cells with **1** resulted in increases in protein expression of cyclin B1 and securing (Figures 5C,D).

Upregulation of the Mitotic Spindle Checkpoint Protein BubR1 was Associated with a Sustained G2/M Cell Cycle Arrest after Treatment with 1. The mitotic spindle checkpoint protein BubR1 has been shown to monitor tension across attached kinetochores and initiate mitotic arrest in response to loss of microtubule tension. As shown in Figure 6A, upregulation of BubR1 was predominantly found in cells treated with 10 μM of **1** for the indicated durations. BubR1
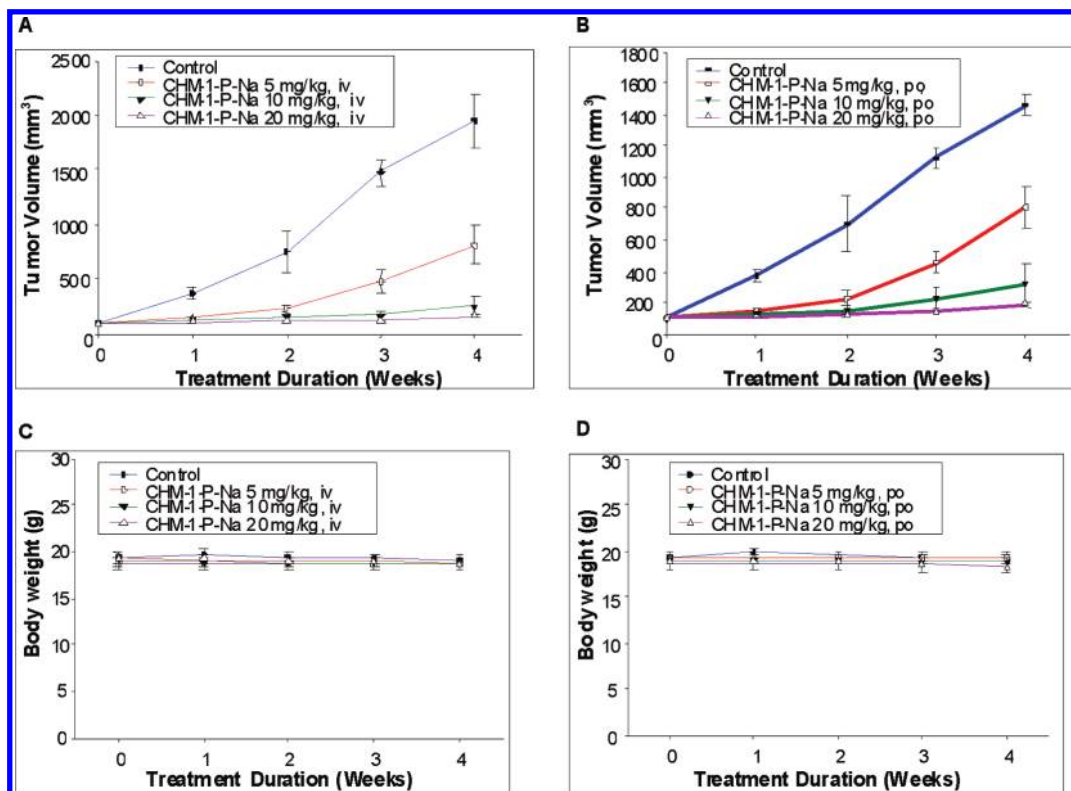
Figure 4. (A) Mean tumor volume−time profiles in SKOV-3 xenograft nude mice ($n = 11$) following iv dosing of **4** at 5, 10, and 20 mg/kg five days per week for four consecutive weeks. (B) Mean tumor volume−time profiles in SKOV-3 xenograft nude mice ($n = 11$) following po dosing of **4** at 5, 10, and 20 mg/kg five days per week for four consecutive weeks. (C) Mean body weight−time profiles in SKOV-3 xeno-graft nude mice ($n = 11$) following iv dosing of **4** at 5, 10, and 20 mg/kg five days per week for four consecutive weeks. (D) Mean body weight−time profiles in SKOV-3 xenograft nude mice ($n = 11$) following po dosing of **4** at 5, 10, and 20 mg/kg five days per week for four consecutive weeks.
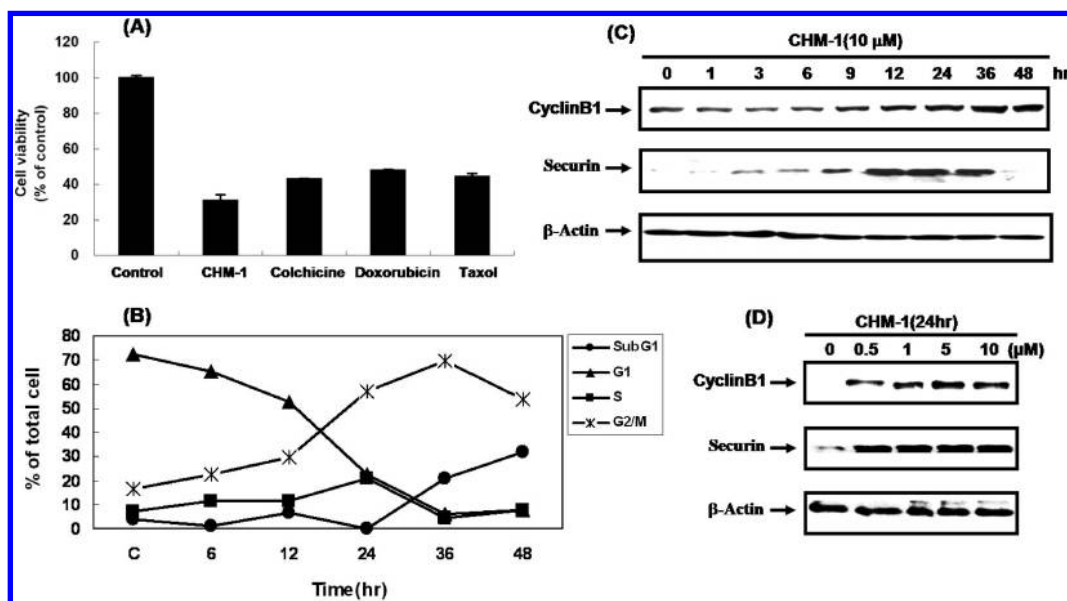
Figure 5. Effect of **1** on cell growth and cell cycle progression in human ovarian cancer cells. (A) SKOV-3 cells were incubated in the absence or presence of the 10 μM of **1**, colchicine, doxorubicin, and taxol for 24 h. (B) The time effect of **1** on cell cycle distribution, cells were treated with 10 μM of **1** for 6, 12, 24, 36, and 48 h and analyzed for propidium iodide-stained DNA content by flow cytometry. (C) SKOV-3 cells were treated with vehicle (DMSO), **1** (10 μM) for the indicated time. (D) SKOV-3 cells were treated with the indicated dose **1** for 24 h. Cells were then harvested and lysed for the detection of cyclin B1, securin, and β-actin protein expression. Western blot data presented are representative of those obtained in at least three separate experiments.

upregulation produced microtubule disruption, as indicated by a significant increase in the percentage of cells arrested in the G2/M phase of the cell cycle (Figure 6B). Moreover, **1** caused the accumulation of BuBR1 (Figure 6B). Our result
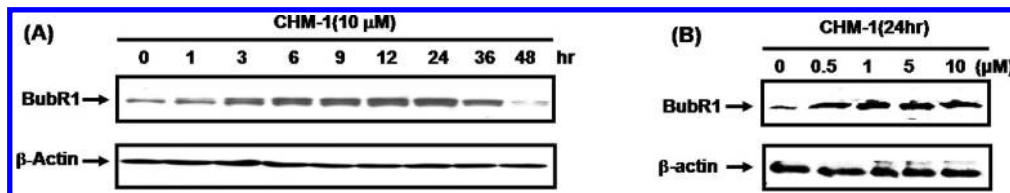
Figure 6. BubR1 upregulation was associated with **1**-induced G2/M cell cycle arrest in human ovarian cancer cells. (A) SKOV-3 cells were treated with vehicle (DMSO), **1** (10 μM) for the indicated time. (B) SKOV-3 cells were treated with the indicated dose **1** for 24 h. Whole-cell lysates were resolved by SDS-PAGE and probed with anti-BubR1 mouse mAb. Results are representative of three separate experiments. Blots were probed with anti-β-actin mAb as a loading control.

suggested that BubR1 contributed to the mitotic checkpoint induced by **1**.

Results and Discussion

As we mentioned earlier, although **1** shows significant antitumor activity with an interesting mechanism of action, its low hydrophilicity limits its development. In this study, we successfully synthesized the monosodium phosphate salt (**4**) of **1**, which could be administrated through oral and iv routes instead of the original ip dosing. The single dose pharmacokinetic study of **4** in male CD-1 mouse proved that **4** was rapidly converted to its active form of **1** via iv or oral administration. By comparing the pharmacokinetic parameters, we postulated that the same dosing of **4** by iv or po routes would result in superior antitumor activity compared with ip dosing of **1**. This postulate was confirmed in the later in vivo antitumor assay. All of these results demonstrated the success of our prodrug strategy, which may highly improve the clinical usage of our drug candidate **1**.

Because **4** was rapidly converted to metabolites in mice with both iv and po administration, we presumed that the antitumor activity of **4** may depend on the overall plasma exposure of **3** and its metabolites. However, comparison of the data in Table 1 revealed a big difference between the total AUC values (measured as the sum of plasma exposure of **1** and **3**) determined after iv and po administration. Nevertheless, the in vivo antitumor activity test results revealed similar antitumor activity between **4** administered via iv and po routes. The dose-dependency of pharmacokinetics versus pharmacodynamic response appears to be nonlinear. Therefore, the contributions from factors such as protein binding, drug distribution, and the possible presence of additional active metabolites need to be further investigated.

The growth inhibition assay of **1** revealed that this compound was particularly active against breast cancer (U251), lung cancer (NCI-H522, DMS273, DMS114), colon cancer (HCT-15, HCT-116), ovarian cancer (OVCAR-4, SKOV-3), stomach cancer (MKN1, MKN7, MKN45), and prostate cancer (DU-145, PC-3). Compound **1** displayed a significant growth inhibition and apoptosis in breast carcinoma cells and promising antitumor actions against human ovarian carcinoma cells compared with those of taxol, colchicine, and doxorubicin.

In our mechanism of action studies of **1**, we observed multiple functions, including antimitotic activity, apoptosis-induction, antimetastasis, and antiangiogenesis.[39] Of particular interest to us is that **1** causes mitotic arrest through the expression of mitotic kinase BubR-1 and disrupts microtubule organization by enhancing SIRT2-mediated tubulin deacetylation. It has been widely reported that cyclin B1/CDK1 complexes are involved in the regulation of the G2/M phase and the M-phase transition. Many reports have demonstrated

that antimicrotubule drug induced M-phase arrest, and inappropriate accumulation of B-type cyclins were associated with the initiation of apoptotic pathways. In this study, **1** arrested the growth of cancer cells at the G2-M phase and then induced apoptotic cell death via the accumulation of cyclin B1. More importantly, the endogenous levels of the mitotic spindle checkpoint protein BubR1 directly correlated with the cellular response to microtubule disruption. The mitotic spindle checkpoint is a complex pathway conserved across species and monitors the metaphase to anaphase transition. The basic model for the spindle checkpoint defines that tension defects or unattached chromosomes activate the checkpoint, delaying the onset of anaphase until such aberrations are corrected.

In this study, our results suggested that absolute levels of BubR1 may determine the length of stay in G2/M. In support of our hypothesis, a recent study demonstrated that knockdown of BubR1 accelerates the normal progression of mitosis.[40] Furthermore, in our study, the **1**-induced G2/M block was maintained until endogenous levels of BubR1 protein became undetectable, and at this point, a marked increase in apoptosis was observed. BubR1 cellular levels inversely correlated with the onset of apoptosis. Collectively, these results suggest that endogenous levels of BubR1 may predict the apoptotic efficacy and potential chemotherapeutic benefit of microtubule-targeted drugs in human cancers. Because the current antimitotic anticancer drugs, such as vinca alkaloids and taxoids, are not cost-effective to synthesize due to structural complexity, **4** represents a promising novel class of mitotic-arresting compounds, which may supplement current cancer chemotherapy.

In conclusion, we have reported the synthesis of the monosodium phosphate prodrug (**4**) of **1** in high yield. Prodrug **4** was readily converted to its parent molecule **1** during both iv and po administration, and showed excellent antitumor activity when administered via iv and po routes to nude mice bearing SKOV-3 xenograft. Results from SPP using enzyme and radioligand binding assays suggested that **4** has clear-cut pharmacological effects on several tumor-associated enzymes and ligands. Further mechanism of action study indicated that **1** arrested the growth of cancer cells at the G2-M phase and then induced apoptotic cell death via the accumulation of cyclin B1. The **1**-induced G2/M block was maintained until endogenous levels of BubR1 protein became undetectable. On the basis of the above findings, we conclude that **4** is a promising anticancer clinical trials candidate, which functions as a novel antimitotic agent.

Experimental Section

Materials. Compounds **1** and **4** were synthesized according to Figure 1B. Melting points were determined with a Yanaco MP-500D melting point apparatus and are uncorrected. IR spectra

were recorded on Shimadzu IRPrestige-21 spectrophotometers as KBr pellets. NMR spectra were obtained on a Bruker Avance DPX-300 FT-NMR spectrometer in $CDCl_3$ or DMSO. The following abbreviations are used: s, singlet; d, doublet; t, triplet; dd, double doublet; and m, multiplet. MS spectra were measured with a Waters Quattro Micro LC/MS/MS instrument. Elemental analyses (C, H, and N) were performed on a Perkin-Elmer 2400 Series II CHNS/O analyzer, and the results were within ±0.4% of the calculated values. HPLC purity analysis of target compound **4** confirmed purity was 99.77%.

Dibenzyl 2-(2-Fluorophenyl)-6,7-methylenedioxyquinolin-4-yl Phosphate (2). Sodium hydride (13.7 mg, 0.57 mmol) was added at 0 °C to a stirred solution of **1** (64.5 mg, 0.23 mmol) in dry THF (10 mL). After 1 h, tetrabenzyl pyrophosphate (**1**) (100 mg, 0.19 mmol) was added and stirring was continued for 20 min. The mixture was filtered and washed with CH_2Cl_2. Then the filtrate was concentrated under vacuum at a temperature below 35 °C. The residue was purified by column chromatography (silica gel, EtOAc/*n*-hexane) to give **2** (69.1 mg, 0.127 mmol). Yield: 67%; mp 101−104 °C. MS (ESI): m/z (M + H)$^+$ 544. ^{1}H NMR ($CDCl_3$, 300 MHz): δ 5.20 (s, 2H), 5.26 (s, 2H), 6.12 (s, 2H), 7.05 (s, 1H), 7.16−7.43 (m, 14H), 7.77 (s, 1H), 8.01−8.02 (m, 1H). Anal. ($C_{30}H_{23}FNO_6P$) C, H, N.

2-(2-Fluorophenyl)-6,7-methylenedioxyquinolin-4-yl Dihydrogen Phosphate (3). A suspension of **2** (97.7 mg, 0.18 mmol) in anhydrous MeOH (10 mL) was hydrogenated in the presence of 10% Pd/C (50 mg) at rt for 10 min. The catalyst and precipitate were collected and dissolved in 10% $NaHCO_3$ solution and then filtered. The filtrate was acidified with diluted aq HCl, and the solid was then collected by filtration and washed with acetone to give **3** (63.5 mg, 0.175 mmol). Yield: 97.2%; mp > 300 °C. MS (ESI): m/z 362 (M − H)$^-$. ^{1}H NMR (DMSO-d_6, 300 MHz): δ 6.22 (s, 2H), 7.32−7.41 (m, 4H), 7.49−7.54 (m, 1H), 7.74 (s, 1H), 7.93−7.98 (m, 1H). Anal. ($C_{16}H_{11}FNO_6P$) C, H, N.

Sodium 2-(2-Fluorophenyl)-6,7-methylenedioxyquinolin-4-yl Hydrogen Phosphate (4). To a flask containing **3** (3.6 g, 10 mmol), a precooled (ice bath) solution of $NaHCO_3$ (0.1 M solution in H_2O, 100 mL) was added dropwise. After the addition was complete, the reaction mixture was removed from the ice bath, stirred at rt for 5 min, and then filtered through celite after no dissolution from the solid was observed. The resulting yellow solution was poured into acetone (400 mL) and kept in an ice bath for 1 h. The precipitate was filtered and washed with ice-cooled acetone (20 mL × 4). The solid was dried under vacuum to yield **4** (2.9 g, 7.5 mmol). Yield: 75.3%; mp > 300 °C. MS(ESI): m/z 384 (M − H)$^-$. ^{1}H NMR (D_2O, 300 MHz): δ 6.22 (s, 2H), 7.23−7.34 (m, 3H), 7.45−7.49 (m, 1H), 7.61 (s, 1H), 7.64 (s, 1H), 7.70 (t, J = 8.1 Hz, 1H). Anal. ($C_{16}H_{10}FNNaO_6P$) C, H, N. HPLC purity analysis. Column: BEH Shield RP18 1.7 μm. Mobile phase: 0.01 M ammonium formate/CAN=80/20. Detection wavelength: PDA Ch1 254 nm at 1.2 mm. Retention time: 0.565 min. Flow rate: 0.4 mL/min. Purity: 99.77%.

Growth Inhibitory Activity of 1 against Human Cancer Cell Line Panel. The system was developed according to the NCI method,[41,42] modified by the Japanese Foundation for Cancer Research (JFCR).[32,43] The cancer panel experiment for **1** was carried out by JFCR, and the inhibition profile was compared with those of more than 300 standard compounds, including various anticancer drugs. The precise experimental method and data analyses have been described elsewhere.[43]

Briefly, we describe the cell lines used and the method for detecting growth inhibition. The following human cancer cell lines were used in cancer panel experiments: breast cancer HBC-4, BSY-1, HBC-5, MCF-7, and MDA-MB-231; brain cancer U251, SF-268, SF-295, SF-539, SNB-75, and SNB-78; colon cancer HCC2998, KM-12, HT-29, HCT-15, and HCT-116; lung cancer NCI-H23, NCI-H226, NCI-H522, NCI-H460, A549, DMS273, and DMS114; melanoma LOX-IMVI; ovarian cancer OVCAR-3, OVCAR-4, OVCAR-5, OVCAR-8, and SKOV-3;

renal cancer RXF-631 L and ACHN; stomach cancer St-4, MKN1, MKN7, MKN28, MKN45, and MKN74; prostate cancer DU-145 and PC-3. The cell lines were cultured in RPMI-1640 (GIBCO/BRL, NY) supplemented with 5% fetal bovine serum (FBS; GIBCO/BRL), penicillin (100 units/mL) (GIBCO/BRL), and streptomycin (100 mg/mL) (GIBCO/BRL) at 37 °C in humidified air containing 5% CO_2. Dose−response curves at five different concentrations between 10^{-4} and 10^{-8} M were obtained from computer analysis. The 50% growth inhibition (GI_{50}), total growth inhibition (TGI), and 50% lethal concentration (LC_{50}) values for these cell lines were determined using the sulforhodamine B (SRB) colorimetric method. Computer processing of these values produced differential activity patterns against the cell lines (mean graphs). The mean graph was compared with those of standard compounds, including various anticancer drugs by using COMPARE analysis.

Single Dose Pharmacokinetics of 4 in Male CD-1 (*Crl.*) Mouse. a. Preparation of Dosing Formulations. Compound **1** was dissolved in cremophor/DMSO/saline (20/5/75, v/v) to make a dosing solution of 2 mg/mL for ip administration. **4** was dissolved in 9% $NaHCO_3$/water to make a dosing solution of 1 mg/mL for iv and oral administration.

b. In Vivo Experiment. Male CD-1 (*Crl.*) mice (body weight: 22−24 g) were used in this study. Source of animals was BioLasco Taiwan. Water was provided ad libitum, regardless of administration route. The **1** solutions (2 mg/mL) were injected ip with a bolus dosing volume of 0.11−0.12 mL (5 mL/kg) per animal. For iv administration, **4** was administered via tail vein with a bolus dosing volume of 0.22−0.24 mL per animal (10 mL/kg). For oral dosing, the drug suspension was given via oral gavages with a dosing volume of 0.22−0.24 mL per animal (10 mL/kg). The animals were fasted for 4 h prior to oral administration and allowed access to standard chow 4 h postdosing.

c. Sample Collection. Each blood sample (0.5−0.7 mL) was collected by decapitation and collected in a prechilling 1.5 mL size Eppendorf safe-lock microcentrifuge tube containing sodium fluoride, followed by centrifugation (12000 rpm, 4 °C) for 10 min. The plasma fraction was transferred to a clean microcentrifuge tube and stored at −70 °C for further analysis. The sampling time points were 0, 5, 15, 30 min, 1, 1.5, 2, 4, 6, 9, 24, and 27 h after ip dosing. The sampling time points were 0, 2, 5, 15, 30 min, 1, 1.5, 2, 4, 6, 9, 24, and 27 h after iv dosing. For oral administration, the blood samples were collected at pre-dose, 15, 30 min, 1, 1.5, 2, 4, 6, 9, 24, and 27 h after dosing. Three mice were used per time point.

d. Analytics and Pharmacokinetic Calculation. The plasma concentrations of **1** and **3** were measured by LC-MS/MS (mass spectrometer: Micromass Quattro Ultima; pump and autosampler: Waters Alliance 2795 LC; data processor: MassLynx version 3.5) method with a reversed-phase Biosil Pro-ODS column. The plasma samples were mixed with acetonitrile, centrifuged, and the supernatant was injected onto an LC column. HPLC conditions were the following. Mobile phase: CHM-1: 35% CH_3CN + 1.0% HCOOH; CHM-1-P: 30% CH_3CN + 1.0% CH_3COOH. Column: Biosil, ODS 4.6 mm × 150 mm, 5 μ. Flow rate: 1.0 mL/min with a post column split 1/10 to mass. Retention time: CHM-1: 2.96 min; CHM-1-P: 3.78 min. Tandem mass spectrometry was performed with electrospray/positive ionization mode, source temperature 80 °C, deesolvation temperature 400 °C. The pharmacokinetic parameters were calculated from mean plasma concentrations by WinNonlin Standard program (version 3.1, Pharsight Corp). The standard curve calculation involved the following: method: simple weighted linear regression with 1 over nominal concentration ($1/x$) or concentration square ($1/x^2$) as weighting factor, response: peak area ratio, equation: $y = bx + a$.

Acute Oral Toxicity Assay. Acute toxicity of **4** was evaluated with the lethal dose test, involving single oral administrations to a group of male and female rats at increasing doses in order to

determine the dose that would kill 50% of mice (LD50) within a set time frame. The assay was conducted in compliance with the Good Laboratory Practice (GLP) regulations. All procedures were approved by the DCB Institutional Animal Care and Use Committee (IACUC) and conducted in compliance with the Guide for the Care and Use of Laboratory Animals.

Fifty SD rats (25 males and 25 females) were obtained from BioLASCO Taiwan Co., Ltd. The rats were approximately 7−8 weeks old at time of dosing. The body weight range was 170−250 g for males and 150−210 g for females.

Rats were randomized into five groups, each consisting of five males and five females. The animals were fasted overnight before dosing. The treated rats were administered test article solution by gavage at dose levels of 500, 1500, 2700, and 5000 mg/kg; the control rats were administered water by gavage with dose volume 20 mL/kg once. Test article solutions were freshly prepared with water for oral injection. Rats were observed once daily for clinical signs of toxicity and twice daily for moribundity/mortality. Body weights were recorded weekly and at necropsy. All animals were euthanized and necropsied for gross lesion examination.

In Vivo Antitumor Activity Assay. Female BALB/c nude mice (18−20 g; 6−8 weeks of age) were purchased from the National Animal Center and maintained in pressurized ventilated cages according to institutional regulations.

SKOV-3, human ovarian cancer cells, were cultured in DMEM/F12 in 10% heat-inactivated bovine serum (FBS) and incubated at 37 °C in humidified atmosphere containing 5% CO_2.

Nude mice were subcutaneously inoculated with SKOV-3 cells at 3×10^6 cells per mouse in 0.5 mL PBS via a 24 gauge needle. After appearance of a 100 mm^3 tumor nodule, 88 tumor-bearing mice were randomly divided into eight groups for treatment with vehicle (PBS) or **4** with different administered methods and doses.

Animals were weighed and tumors were measured using calipers twice weekly before, during, and after drug treatments. Tumor volume was calculated with the following formula: $^1/_2(L + W^2)$, where L is the length and W is the width.[44,45] At the end of the experiments, animals were euthanized with carbon dioxide followed by cervical dislocation. The tumors were excised, weighed, and sectioned, and the tumor sections were embedded in OCT compound and frozen at −70 °C.

a. . The mice were administered with single intravenous dosing of **4** via tail vein five days per week for four consecutive weeks at 5, 10, and 20 mg/kg.

b. . The mice were administered with single oral dosing of **4** five days per week for four consecutive weeks at 5, 10, and 20 mg/kg.

Enzyme Assay and Radioligand Binding Assay (Spectrum Screen).[46] MDS PharmaServices performed this testing under standard protocols.

Mechanism of Action Study. a. Antibodies and Reagents. Antibodies and reagents were purchased from commercial sources: antibodies against cyclin B1 and securing were purchased from Cell Signaling Technology (Beverly, MA); antibody against BuBR1 was from BD Biosciences (Los Angeles, CA); antimouse and antirabbit antibodies conjugated to horseradish peroxidase were obtained from Santa Cruz Biotechnology (Santa Cruz, CA); β-actin antibody and PI were from Sigma Chemical Co. (St. Louis, MO).

b. Cell Lines and Cell Cultures. The human ovarian cancer cell line SKOV-3 was obtained from The American Type Culture Collection (Rockville, MD) and propagated in 100 mm culture dishes at the desired density in DMEM/F-12 supplemented with 10% fetal calf serum and 1% penicillin−streptomycin. These cells were grown at 37 °C in a humidified atmosphere of 5% CO_2.

c. Western Blot Analyses. Cells (1×10^6) were washed twice with PBS, and then the gold lysis buffer (10% glycerol, 1%

Triton X-100, 1 mM PMSF, 10 μg/mL leupeptin, 1 mM sodium orthovanadate, 1 mM EGTA, 10 mM NaF, 1 mM sodium pyrophosphate, 100 mM β-glycerophosphate, 20 mM Tris-HCl, 137 mM NaCl, 5 mM EDTA, 0.1% sodium dodecyl sulfate, and 10 μg/mL aprotinin. Adjust pH to 7.9) was added to lyse the cells. After the cells lysed, the suspension solution were centrifuged, and the Bio-Rad protein assay kit (Bio-Red Laboratories) was used to determine the protein contents. Taken were 50 μg proteins to be resolved with SDS-PAGE and transferred to PVDF membrane (polyvinylidene fluoride transfer membrane) (BioTrace, UK.). The membrane was blocked by blocking buffer (nonfat milk 5%), NaN_3 (0.2%), and Tween 20 (0.2%, v/v) in TBS. Then the PVDF membrane was incubated with primary antibodies, followed by incubation with horseradish peroxidase-conjugated goat antimouse antibody (1:2500 dilution, Roche Applied Science, Indianapolis, IN). Reactive bands were visualized with an enhanced chemiluminescence system (Amersham Biosciences, Arlington Heights, IL). The intensity of the bands was scanned and quantified with a Phosphor-Image system.

d. Cell Proliferation Assays. Cells (1×10^4) were seeded on the 24-well cell culture cluster overnight and then treated with indicated drug and incubated for 24 h. Next, 40 μL of MTT (3-(4,5-dimethylthiazol-2-yl)-2,5-diphenyl tetrazolium bromide) (stock conc 2 mg/mL, Sigma Chemical Co.) was added to each well (volume of each well was 500 μL) and then incubated for 2 h at 37 °C. After MTT-formazan crystals were formed, 250 μL of DMSO was added to dissolve the crystals. Finally, absorbance was detected at O.D. 550 nm by an enzyme-linked immunosorbent assay (ELISA) reader.

e. Flow Cytometry. The cell cycle analysis was determined by flow cytometry. Cells were cultured in 60 mm Petri dishes and incubated for various times. After being trypsinized and washed twice with ice-cold PBS, the cells were fixed with 70% ice-cold EtOH overnight at −20 °C. After centrifugation, the cell pellets were treated with RNAase A and exposed to PI and then analyzed by flow cytometry (FACScan, BD Biosciences, Mountain View, CA). The percentage was analyzed by Cell Quest software (BD Biosciences).

Supporting Information Available: Literature references for spectrum screen (enzyme and radioligand binding assays); analytical results. This material is available free of charge via the Internet at http://pubs.acs.org.

References

(1) Kuo, S. C.; Lee, H. Z.; Juang, J. P.; Lin, Y. T.; Wu, T. S.; Chang, J. J.; Lednicer, D.; Paull, K. D.; Lin, C. M. Synthesis and cytotoxicity of 1,6,7,8-substituted-2-(4′-substituted phenyl)-4-quinolones and related compounds: identification as antimitotic agents interacting with tubulin. *J. Med. Chem.* **1993**, *36* (9), 1146–1156.

(2) Li, L.; Wang, H. K.; Kuo, S. C.; Wu, T. S.; Lednicer, D.; Lin, C. M.; Hamel, E.; Lee, K. H. Antitumor agents. 150. 2′,3′,4′,5′,5,6,7-Substituted 2-phenyl-4-quinolones and related compounds: their synthesis, cytotoxicity, and inhibition of tubulin polymerization. *J. Med. Chem.* **1994**, *37* (8), 1126–1135.

(3) Li, L.; Wang, H. K.; Kuo, S. C.; Wu, T. S.; Mauger, A.; Lin, C. M.; Hamel, E.; Lee, K. H. Antitumor agents. 155. Synthesis and biological evaluation of 3′,6,7-substituted 2-phenyl-4-quinolones as antimicrotubule agents. *J. Med. Chem.* **1994**, *37* (20), 3400–3407.

(4) Chen, K.; Kuo, S. C.; Hsieh, M. C.; Mauger, A.; Lin, C. M.; Hamel, E.; Lee, K. H. Antitumor agents. 174. 2′,3′,4′,5,6,7-Substituted 2-phenyl-1,8-naphthyridin-4-ones: their synthesis, cytotoxicity, and inhibition of tubulin polymerization. *J. Med. Chem.* **1997**, *40* (14), 2266–2275.

(5) Chen, K.; Kuo, S. C.; Hsieh, M. C.; Mauger, A.; Lin, C. M.; Hamel, E.; Lee, K. H. Antitumor agents. 178. Synthesis and biological evaluation of substituted 2-aryl-1,8-naphthyridin-4(1*H*)-ones as antitumor agents that inhibit tubulin polymerization. *J. Med. Chem.* **1997**, *40* (19), 3049–3056.

(6) Xia, Y.; Yang, Z. Y.; Xia, P.; Bastow, K. F.; Tachibana, Y.; Kuo, S. C.; Hamel, E.; Hackl, T.; Lee, K. H. Antitumor agents. 181. Synthesis and biological evaluation of 6,7,2′,3′,4′-substituted-1,2,3,4-tetrahydro-2-phenyl-4-quinolones as a new class of antimitotic antitumor agents. *J. Med. Chem.* **1998**, *41* (7), 1155–1162.

(7) Zhang, S. X.; Bastow, K. F.; Tachibana, Y.; Kuo, S. C.; Hamel, E.; Mauger, A.; Narayanan, V. L.; Lee, K. H. Antitumor agents. 196. Substituted 2-thienyl-1,8-naphthyridin-4-ones: their synthesis, cytotoxicity, and inhibition of tubulin polymerization. *J. Med. Chem.* **1999**, *42* (20), 4081–4087.

(8) Zhang, S. X.; Feng, J.; Kuo, S. C.; Brossi, A.; Hamel, E.; Tropsha, A.; Lee, K. H. Antitumor agents. 199. Three-dimensional quantitative structure−activity relationship study of the colchicines binding site ligands using comparative molecular field analysis. *J. Med. Chem.* **2000**, *43* (2), 167–176.

(9) Hour, M. J.; Huang, L. J.; Kuo, S. C.; Xia, Y.; Bastow, K.; Nakanishi, Y.; Hamel, E.; Lee, K. H. 6-Alkylamino- and 2,3-dihydro-3′-methoxy-2-phenyl-4-quinazolinones and related compounds: their synthesis, cytotoxicty, and inhibition of tubulin polymerization. *J. Med. Chem.* **2000**, *43* (23), 4479–4487.

(10) Xia, Y.; Yang, Z. Y.; Xia, P.; Hackl, T.; Hamel, E.; Mauger, A.; Wu, J. H.; Lee, K. H. Antitumor agents. 211. Fluorinated 2-phenyl-4-quinolone derivatives as antimitotic antitumor agents. *J. Med. Chem.* **2001**, *44* (23), 3932–3936.

(11) Xia, T.; Yang, Z. Y.; Hour, M. J.; Kuo, S. C.; Xia, P.; Bastow, K. F.; Nakanishi, Y.; Nampoothiri, P.; Hackl, T.; Hamel, E.; Lee, K. H. Antitumor agents. Part 204: Synthesis and biological evaluation of substituted 2-aryl quinazolinones. *Bioorg. Med. Chem. Lett.* **2001**, *11* (9), 1193–1196.

(12) Xia, T.; Yang, Z. Y.; Xia, P.; Bastow, K. F.; Nakanishi, Y.; Nampoothiri, P.; Hamel, E.; Brossi, A.; Lee, K. H. Antitumor agents. Part 226: Synthesis and cytotoxicity of 2-phenyl-4-quinolone acetic acids and their esters. *Bioorg. Med. Chem. Lett.* **2003**, *13* (17), 2891–2893.

(13) Lai, Y. Y.; Huang, L. J.; Lee, K. H.; Xiao, Z. Y.; Bastow, K. F.; Yamori, T.; Kuo, S. C. Synthesis and biological relationships of 3′,6-substituted 2-phenyl-4-quinolone-3-carboxylic acid derivatives as antimitotic agents. *Bioorg. Med. Chem.* **2005**, *13* (1), 265–275.

(14) Nakamura, S; Kozuka, M.; Bastow, K. F.; Tokuda, H.; Nishino, H.; Suzuki, M.; Tatsuzaki, J.; Morris-Natschke, S. L.; Kuo, S. C.; Lee, K. H. Cancer preventive agents, Part 2: Synthesis and evaluation of 2-phenyl-4-quinolone and 9-oxo-9,10-dihydroacridine derivatives as novel antitumor promoters. *Bioorg. Med. Chem.* **2005**, *13* (14), 4396–4401.

(15) Wang, S. W.; Pan, S. L.; Huang, Y. C.; Guh, J. H.; Chiang, P. C.; Huang, D. Y; Kuo, S. C.; Lee, K. H.; Teng, C. M. CHM-1, a novel synthetic quinolone with potent and selective antimitotic antitumor activity against human hepatocellular carcinoma in vitro and in vivo. *Mol. Cancer Ther.* **2008**, *7* (2), 350–360.

(16) Heimbach, T; Oh, D. M.; Li, L. Y.; Forsberg, M.; Savolainen, J.; Leppänen, J.; Matsunaga, Y.; Flynn, G.; Fleisher, D. Absorption rate limit considerations for oral phosphate prodrug. *Pharm. Res.* **2003**, *20* (6), 848–856.

(17) Jordan, M. A. Mechanisms of action of antitumor drugs that interact with microtubules and tubulin. *Curr. Med. Chem. Anticancer Agents* **2002**, *2*, 1–17.

(18) Casagrande, C.; Merlo, L.; Ferrini, R.; Miragoli, G.; Semeraro, C. Cardiovascular and renal action of dopaminergic prodrugs. *J. Cardiovasc. Pharmacol.* **1989**, *14*, S40–S59.

(19) Juntunen, J.; Huuskonen, J.; Laine, K.; Niemi, R.; Taipale, H.; Nevalainen, T.; Pate, D. W.; Järvinen, T. Anandamide prodrugs 1. Water-soluble phosphate esters of arachidonylethanolamide and R-methanandamide. *Eur. J. Pharm. Sci.* **2003**, *19* (1), 37–43.

(20) Pettit, G. R.; Grealish, M. P.; Jung, M. K.; Hamel, E.; Pettit, R. K.; Chapuis, J. C.; Schmidt, J. M. Antineoplastic agents. 465. Structural modification of resveratrol: sodium resverastatin phosphate. *J. Med. Chem.* **2002**, *45* (12), 2534–2542.

(21) Perry, C. M.; McTavish, D. Estramustine phosphate sodium. A review of its pharmacodynamic and pharmacokinetic properties, and therapeutic efficacy in prostate cancer. *Drugs Aging* **1995**, *7* (1), 49–74.

(22) Witterland, A. H. I.; Koks, C. H. W.; Beijnen, J. H. Etoposide phosphate, the water soluble prodrug of etoposide. *Pharm. World Sci.* **1996**, *18*, 163–170.

(23) Vincent, L.; Kermani, P.; Young, L. M.; Cheng, J.; Fan, Z.; Shido, K.; Lam, G.; Bompais-Vincent, H.; Zhu, Z.; Hicklin, D. J.; Bohlen, P.; Chaplin, D. J.; May, C.; Rafii, S. Combretastatin A4 phosphate induces rapid regression of tumor neovessels and growth through interference with vascular endothelial-cadherin signaling. *J. Clin. Invest.* **2005**, *115* (11), 2992–3006.

(24) Pettit, G. R.; Temple, C.; Narayanan, V. L.; Varma, R.; Simpson, M. J.; Boyd, M. R.; Rener, G. A.; Bansal, N. Antineoplastic agents 322. Synthesis of combretastatin A-4 prodrugs. *Anti-Cancer Drug Des.* **1995**, *10* (4), 299–309.

(25) Edsall, A.; Agoston, G.; Treston, A.; Plum, S.; McClanahan, R.; Lu, J.; Song, W.; Cushman, M. Synthesis and in vivo antitumor evaluation of 2-methoxyestradiol 3-phosphate, 17-phosphate, and 3,17-diphosphate. *J. Med. Chem.* **2007**, *50* (26), 6700–6705.

(26) Ho, N. H.; Harapanhalli, R. S.; Dahman, B. A.; Chen, K.; Wang, K.; Adelstein, S. J.; Kassis, A. I. Synthesis and biologic evaluation of a radioiodinated quinazolinone derivative for enzyme-mediated insolubilization therapy. *Bioconjugate Chem.* **2002**, *13* (2), 357–364.

(27) Chen, K; Wang, K; Kirichian, A. M.; Al Aowad, A. F.; Iyer, L. K.; Adelstein, S. J.; Kassis, A. I. In silico design, synthesis, and biological evaluation of radioiodinated quinazolinone derivatives for alkaline phosphatase-mediated cancer diagnosis and therapy. *Mol. Cancer Ther.* **2006**, *5* (12), 3001–3013.

(28) Pososil, P.; Wang, K.; Al Aowad, A. F.; Iyer, L. K.; Adelstein, S. J.; Kassis, A. I. Computational modeling and experimental evaluation of a novel prodrug for targeting the extracellular space of prostate tumors. *Cancer Res.* **2007**, *67*, 2197–2205.

(29) Wang, K.; Kirichian, A. M.; Al Aowad, A. F.; Adelstein, S. J.; Kassis, A. I. Evaluation of chemical, physical, and biologic properties of tumor-targeting radioiodinated quinazolinone derivative. *Bioconjugate Chem.* **2007**, *18*, 754–764.

(30) Andrews, K. J. M.; Atherton, F. R.; Bergel, F.; Morrison, A. L. Hydroxypyridine and hydroxyquinoline phosphates as anticholinesterases. *J. Chem. Soc.* **1954**, 1638–1640.

(31) Horst, G.; Harald, K.; Hilmar, M.; Gerhard, S. New 4-quinolinol- and 5,6,7,8-tetrahydro-4-quinolinol derivatives with biocidal effect. *Liebigs Ann. Chem.* **1982**, 1656–1676.

(32) Yamori, T.; Matsunaga, A.; Sato, S.; Yamazaki, K.; Komi, A.; Ishizu, K.; Mita, I.; Edatsugi, H.; Matsuba, Y.; Takezawa, K.; Nakanishi, O.; Kohno, H.; Nakajima, Y.; Komatsu, H.; Andoh, T.; Tsuruo, T. Potent antitumor activity of MS-247, a novel DNA minor groove binder, evaluated by an in vitro and in vivo human cancer cell line panel. *Cancer Res.* **1999**, *59*, 4042–4049.

(33) Yaguchi, S.; Fukui, Y.; Koshimizu, I.; Yoshimi, H.; Matsuno, T.; Gouda, H.; Hirono, S.; Yamazaki, K.; Yamori, T. Antitumor activity of ZSTK474, a new phosphatidylinositol 3-kinase inhibitor. *J. Natl. Cancer Inst.* **2006**, *98* (8), 545–556.

(34) Radke, I.; Gotte, M.; Kersting, C.; Mattsson, B.; Kiesel, L.; Wulfing, P. Expression and prognostic impact of the protein tyrosine phosphatases PRL-1, PRL-2, and PRL-3 in breast cancer. *Br. J. Cancer* **2006**, *95* (3), 347–354.

(35) Rochefort, H.; Garcia, M.; Glondu, M.; Laurent, V.; Liaudet, E.; Rey, J.-M.; Roger, P. Cathepsin D in breast cancer: mechanisms and clinical application, a 1999 overview. *Clin. Chim. Acta* **2000**, *291* (2), 157–170.

(36) Liaudet-Coopman, E.; Beaujouin, M.; Derocq, D.; Garcia, M.; Glondu-Lassis, M.; Laurent-Matha, V.; Prébois, C.; Rochefort, H.; Vignon, F. Cathepsin D: newly discovered functions of a long-standing aspartic protease in cancer and apoptosis. *Cancer Lett.* **2006**, *237* (2), 167–179.

(37) Chang, W. S.; Wu, H. R.; Yeh, C. T.; Wu, C. W.; Chang, J. Y. Lysosomal cysteine proteinase cathepsin S as a potential target for anti-cancer therapy. *J. Cancer Mol.* **2007**, *3*, 5–14.

(38) Takehara, A.; Hosokawa, M.; Eguchi, H.; Ohigashi, H.; Ishikawa, O.; Nakamura, Y.; Nakagawa, H. γ-Aminobutyric acid (GABA) stimulates pancreatic cancer growth through overexpressing GABA$_A$ receptor π subunit. *Cancer Res.* **2007**, *67*, 9704–9712.

(39) Wang, S. W.; Pan, S. L.; Peng, C. Y.; Huang, D. Y.; Tsai, A. C.; Chang, Y. L.; Guh, J. H.; Kuo, S. C.; Lee, K. H.; Teng, C. M. CHM-1 inhibits hepatocyte growth factor-induced invasion of SK-Hep-1 human hepatocellular carcinoma cells by suppressing matrix metalloproteinase-9 expression. *Cancer Lett.* **2007**, *257*, 87–96.

(40) Meraldi, P.; Draviam, V. M.; Sorger, P. K. Timing and checkpoints in the regulation of mitotic progression. *Dev. Cell* **2004**, *7*, 45–60.

(41) Paull, K. D.; Shoemaker, R. H.; Hodes, L.; Monks, A.; Scudiero, D. A.; Rubinstein, L.; Plowman, J.; Boyd, M. R. Display and analysis of patterns of differential activity of drugs against human tumor cell lines: development of mean graph and COMPARE algorithm. *J. Natl. Cancer Inst.* **1989**, *81* (14), 1088–1092.

(42) Monks, A.; Scudiero, D.; Skehan, P.; Shoemaker, R.; Paull, K.; Vistica, D.; Hose, C.; Langley, J.; Cronise, P.; Vaigro-Wolff, A.; Gray-Goodrich, M.; Campbell, H.; Mayo, J.; Boyd, M. Feasibility

of a high-flux anticancer drug screen using a diverse panel of cultured human tumor cell lines. *J. Natl. Cancer Inst.* **1991**, *83*, 757–766.

(43) Yamori, T. Panel of human cancer cell lines provides valuable database for drug discovery and bioinformatics. *Cancer Chemother. Pharmacol.* **2003**, *52*, S74–S79.

(44) Euhus, D. M.; Hudd, C.; LaRegina, M. C.; Johnson, F. E. Tumor measurement in the nude mouse. *J. Surg. Oncol.* **1986**, *31*, 229–234.

(45) Tomayko, M. M.; Reynolds, C. P. Determination of subcutaneous tumor size in athymic (nude) mice. *Cancer Chemother. Pharmacol.* **1989**, *24*, 148–154.

(46) References provided in Supporting Information.